Int. J. Electrochem. Sci., 10 **(2015)** 1543 - 1554

International Journal of
ELECTROCHEMICAL
SCIENCE
www.electrochemsci.org

Synthesis of Heterocyclic Compounds of 5-substituted-1,3,4-oxadiazole-2-thiols for the Prevention of Nickel Corrosion

Shelly Gapil[1], *Mehdi Ebadi*[2,*], *Wan J. Basirun*[1,3], *Aurangzeb Hasan*[4], *Khalijah Awang*[1,*], *Maziar A. Golsefidi*[5], *Mohamad N. Azmi*[1], *M.Y. Sulaiman*[2].

[1]Department of Chemistry, Faculty of Science, University of Malaya, 50603 Kuala Lumpur, Malaysia.
[2]Solar Energy Research Institute, University Kebangsaan Malaysia, Bangi, Selangor, Malaysia
[3]Institute of Nanotechnology & Catalysis research (NanoCat), University of Malaya, 50603 Kuala Lumpur, Malaysia.
[4]Department of Chemistry, Quaid-i-Azam University, 45320, Islam Abad, Pakistan.
[5]Department of Chemistry, Faculty of Sciences, Islamic Azad University-Gorgan Branch, Gorgan, 49147-39975, Iran.
[*]E-mail: mehdi_2222002@yahoo.com, khalijah@um.edu.my.

Received: 3 August 2014 / *Accepted:* 15 September 2014 / *Published:* 30 December 2014

Two heterocyclic compounds, 5-(4-methoxyphenyl)-1,3,4-oxadiazole-2-thiol (**A1**) and 5-(4-nitrophenyl)-1,3,4-oxadiazole-2-thiol (**A2**) were studied as inhibitors of nickel metal corrosion. The kinetic and thermodynamic parameters of corrosion were determined from polarization curves and impedance measurements. It was found that the nickel surface was protected from corrosion when the inhibitor concentration was increased in the corrosive medium. Electrochemical impedance spectroscopy, open circuit potential, and linear scan voltammetry results showed that the corrosion rate of Ni decreased in the presence of inhibitors in a 3.5% NaCl solution, with the inhibition strength in the order **A1** > **A2**. EIS measurements showed that the charge transfer resistances of the nickel surface in 0.16 mM **A1** and **A2** were 144.2 and 119.3 kΩ cm^2 in a 3.5% NaCl solution, respectively. FESEM images showed that the surface was well protected against corrosion when the concentration of inhibitors was increased to 0.3 mM in the corrosive media.

Keywords: corrosion behavior, nickel, EIS, Polarization measurements, 1,3,4-oxadiazole-2-thiols, organic inhibitor, heterocyclic compound.

1. INTRODUCTION

Five-membered N-containing heterocyclic aromatic compounds found in natural products [1] are of great interest due to their medicinal properties [2]. Purine alkaloids, such as theophylline, are known for their muscle relaxant properties, while another type of terpenoid indole, Ibogaine from

Tabernanthe iboga, is effective against drug addiction [3]. Among heterocyclic compounds, 1,3,4-oxadiazole moieties have shown a significant role in materials science [4] and agrochemistry [5] are widely used as pharmacophores [6]. Hence, it is not surprising that a number of synthesis methods for the preparation of 1,3,4-oxadiazoles have been developed over the years [7].

Due to its excellent properties, nickel is an important metal with a wide range of decorative and industrial applications. Nickel and its alloys are widely used in industry due to their impact strength, toughness, corrosion resistance and friction resistance [8-9]. In addition, metallic nickel, nickel alloys and nickel oxides are used in electronic devices (such as batteries, super-capacitors and electrocatalysis) and as nanosheets, nanowires and nanotubes. To protect nickel and its alloys from corrosion, it is necessary to improve the corrosion resistance of the surface. Occasionally, the metal surface is interfaced with acidic media for pickling, rust removal, *etc*. An alternative method for controlling corrosion processes on metal surfaces is the addition of organic inhibitors. The adsorption of organic inhibitors on metal surfaces occurs *via* nitrogen and oxygen atoms. Sulfur, phosphorus [9-10] and heterocyclic molecules containing N and S atoms have also been investigated by other researchers [11].

Electrochemical techniques are powerful tools for studying the influence of inhibitors on the corrosion resistance of metal surfaces. Electrochemical DC techniques, such as open circuit potential (OCP) and Tafel plots, can provide information about the efficiency of the inhibitors in the corrosive environment. The performance of the inhibitors against corrosion can be determined from corrosion rate measurements under different conditions [12-17]. Electrochemical impedance spectroscopy (EIS) is another powerful tool to investigate the surface of the corroding metal and is complementary to DC methods [18-20]. In the present study, the corrosion behavior of Ni in a 3.5% NaCl solution with different concentrations of **A1** and **A2** was studied using a combination of AC (EIS) and DC methods (OCP and Tafel). These tools represent established techniques for studying the performance of organic inhibitors in corrosive solutions [12].

2. EXPERIMENTAL METHODS

2.1. Synthesis of 5-substituted-1,3,4-oxadiazole-2-thiols (A1 and A2)

The synthetic protocol used for the preparation of 5-(4-methoxyphenyl)-1,3,4-oxadiazole-2-thiol (**A1**) and 5-(4-nitrophenyl)-1,3,4-oxadiazole-2-thiol (**A2**) was previously reported by us [21-22]

2.2. Corrosion characterization techniques

Experiments were performed using Ni foils of 99.9% purity in 3.5% NaCl aqueous media containing varying amounts of inhibitors (0 - 0.16 mM). The Ni foils (0.2× 1× 1 cm) were polished with emery paper (2000 grit), rinsed in distilled water and finally ultrasonicated in acetone to remove oily stains. A three-compartment cell was used in the corrosion measurements with Ni and platinum foils as the working electrode (WE) and counter electrode (CE), respectively, and the reference (RE) was a saturated calomel electrode (SCE). Frequency response analysis (FRA) software was used in the

EIS experimental and simulation process, while general-purpose electrochemical software (GPES) was used in the linear scan voltammetry (LSV, Tafel) and open circuit potential (OCP) techniques. The software programs were installed on a computer interfaced with an Autolab (302 N) potentiostat/galvanostat instrument (Ecochemie, Netherlands). The scan rate for LSV was 1 mV s^{-1}, with a potential range of 0.15 V to −0.65 V. The EIS measurements were carried out with a frequency domain of 100 kHz-10 mHz with an amplitude of 5 mV around the OCP. Prior to all analyses (EIS and LSV), the Ni foils were immersed in the corrosive solution (3.5% NaCl) containing different amounts of inhibitors for 1 hr to obtain the OCP value. The Gaussian 9, was used to calculate the quantum chemical parameters (such as highest occupied molecular orbital –HOMO- and lowest unoccupied molecular orbital- LUMO) of inhibitor through the density function theory (DFT). A JEOL JSM-840A field emission scanning electron microscopy (FESEM) instrument was used to capture the images of the Ni surface after immersion in the corrosive solution for 1 month.

3. RESULTS AND DISCUSSION

3.1. Open circuit potential

The effects of different concentrations of **A1** and **A2** on the OCP of nickel foils in 3.5% NaCl were examined and are displayed in Fig. 1 (a and b). Two notable features can be distinguished in both diagrams. First, it can be observed that the electrode potential shifts to more negative values with time as soon as the Ni foil is immersed in the corrosive media. This suggests that the oxide film dissolves initially before a steady-state condition is achieved [23]. However, El-Dahan *et al*. [24] suggested that this behavior is due to the dissolution of the metal oxide on the anode surface rather than to the formation of metal oxide on the cathode surface. Second, the steady-state potential shifts to noble values with increasing inhibitor concentrations. The increase in OCP towards noble potentials is due to the adsorption of the inhibitor on the nickel surface.

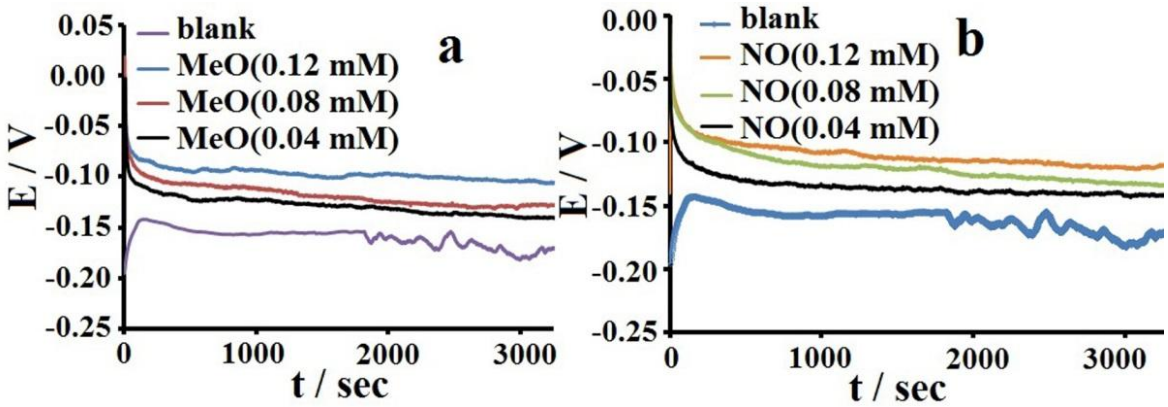

Figure 1. OCP measurements (vs. SCE) as a function of time for nickel plates with different inhibitor concentrations (a: **A1** and b: **A2**) in 3.5% NaCl solution for 1 h.

3.2. Polarization and Frontier Molecular Orbital (FMO) measurements

The corrosion behavior of Ni was studied at various concentrations of **A1** and **A2** in a 3.5% NaCl solution. The cathodic and anodic polarization curves of Ni in varying concentrations (0 – 0.08 mM) of **A1** and **A2** are illustrated in Fig. 2a and 2c, respectively. In addition, the Tafel plots were also studied for Ni with 0.2 mM **A1** (Fig. 2b) and **A2** (Fig. 2d) in a 3.5% NaCl solution at 35, 40 and 45°C. The corrosion potential E_{corr} and corrosion current I_{corr} were determined from the extrapolation of the cathodic and anodic Tafel plots in the linear region at the intersection point for all the curves and are tabulated in Table 1. It was found that the difference between E_{corr} and I_{corr} was due to the presence of the inhibitors. The inhibition efficiency (*IE*%) was calculated from the polarization data *via* Eq. 1.

$$IE\% = \frac{CR^0 - CR}{CR^0} \times 100 \qquad (1)$$

where CR^0 and CR are the corrosion rates in the absence and presence of various amounts of inhibitors, respectively. However, from the Butler–Volmer equation ($CR = 3.27 \times 10^{-3}\ I_{corr}.(E_w)/\rho$), the corrosion rate ($CR$) can be calculated, while I_{corr} can be determined from the intersection of the straight lines of the Tafel cathodic and anodic curves, with the slopes of β_c and β_a, respectively. The parameters E_w and ρ are the equivalent weight and density of the corroding metal, respectively.

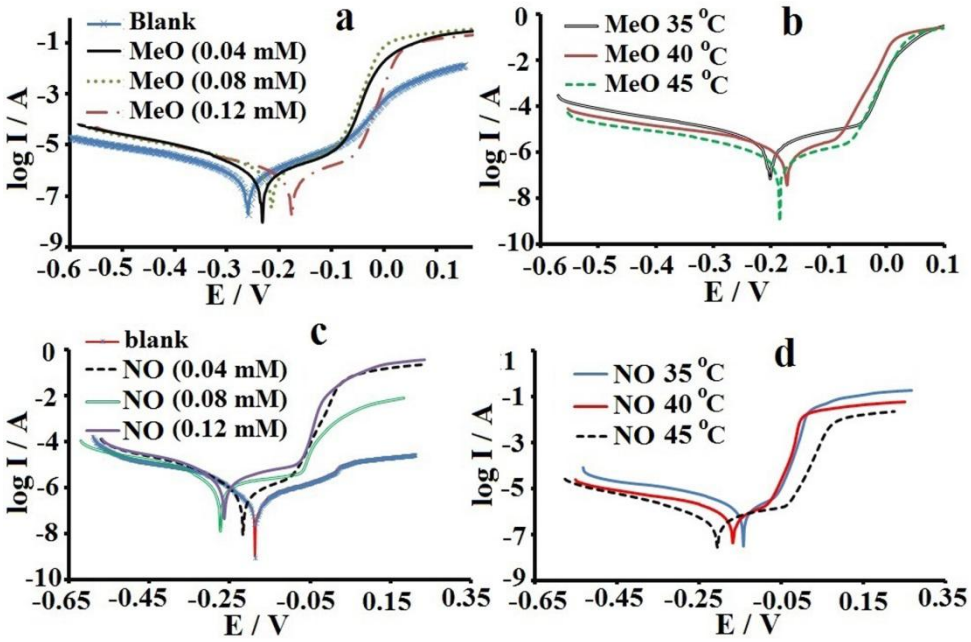

Figure 2. Tafel polarization curves (vs. SCE) for the corrosion of Ni with different concentrations of **A1** and **A2** in 3.5% NaCl. Left side curves in various amounts of **A1** and **A2**: a and c, respectively. The Tafel plots on the right (**A1**: b and **A2**: d) show the corrosion behavior in the presence of 0.2 mM inhibitors at different temperatures.

The active sites could be blocked by increasing the inhibitor concentration. In other words, the surface coverage (θ) increased with increasing inhibitor concentration in the corrosive media. The

surface coverage (θ) is an important factor that can be used to describe the adsorption mechanism of the inhibitors. The most common isotherms used to calculate the surface coverage (θ) are [25]:

Frumkin isotherm: $(\theta/1\text{-}\theta)exp(-2F\theta) = K_{ads}. C$

Freundlich isotherm: $\theta = K_{ads}. C$

Temkin isotherm: $\exp(f.\theta) = K_{ads}. C$

Langmuir isotherm: $(\theta/1\text{-}\theta) = K_{ads}. C$

where $K_{ads.}$ is the equilibrium constant for the adsorption process, C is the inhibitor concentration, and f is the energy inhomogeneity.

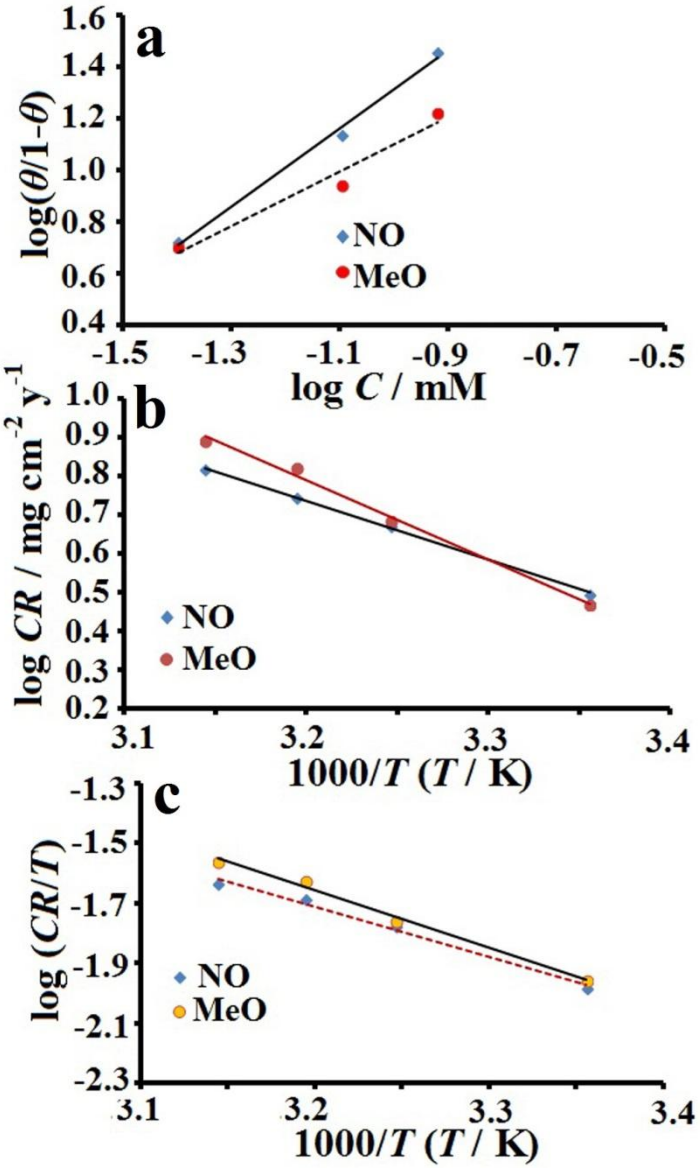

Figure 3. Adsorption isotherm plots in varying concentrations of **A1** and **A2** in a 3.5% NaCl solution, a): log θ/θ-1 vs. log C, b): logCR vs. (1000/T), c): logCR/T vs. (1000/T).

It was found that the Langmuir adsorption isotherm gave the best straight line for the inhibitors (Fig. 2a: log[$\theta/1\text{-}\theta$] *vs.* log C). The calculation of θ is given by eq. 2 [26]:

$$\theta = \frac{C_{Ro} - C_R}{C_{Ro} - C_{Rm}} \quad (2)$$

where C_{Ro}, C_R and C_{Rm} are the corrosion rates of the uninhibited, inhibited and maximally inhibited nickel plates in a 3.5% NaCl solution, respectively. The straight lines in Fig. 3a (log[θ/1-θ] *vs.* log *C*) suggest that the inhibitors at the metal/electrolyte interface follow a Langmuir adsorption isotherm.

Table 1 shows that the surface coverage (θ) increases with increasing inhibitor concentration. In contrast, the surface coverage value decreases (active sites on the Ni surface increases) with increasing temperature. The same results were found by Singh *et al.*, [27] once they have investigated the corrosion behavior of mild steel using different concentration of ceftadizime (CZD) as an inhibitor.

Table 1. Electrochemical kinetic parameters for Ni in the absence and presence of different concentrations of **A1** and **A2** in a 3.5% NaCl solution.

	Conc. Inhib. (mM)	$E_{corr.}$ (mV)	$I_{corr.}$ (A cm^{-2})	β_c (mV/ dec)	β_a (mV/ dec)	R_p (Ω cm^{-2}) $\times10^{+4}$	CR (mm/y)	IE%	$K_{ads.}$ (mol^{-1})	ΔG (kJ mol^{-1})	θ
Blank	0.0	-271	1.1×10^{-6}	387	134	1.97	1.2×10^{-2}	-	-	-	-
A1	0.04	-252	4.8×10^{-7}	101	138	1.507	5.0×10^{-3}	58.3	$13.1\times10^{+4}$	-16941	0.84
	0.08	-193	3.9×10^{-7}	126	119	1.825	3.3×10^{-3}	72.5	$16.3\times10^{+4}$	-14990	0.929
	0.12	-174	3.5×10^{-7}	149	107	2.537	2.7×10^{-3}	77.5	$23.6\times10^{+4}$	-15337	0.966
A2	0.04	-261	4.9×10-7	136	125	1.235	5.2×10-3	56.6	14.8×10+4	-14900	0.856
	0.08	-213	4.1×10-7	95	138	1.637	4.2×10-3	65	10.8×10+4	-14605	0.897
	0.12	-188	2.5×10-7	101	150	1.968	3.7×10-3	69.1	16.9×10+4	-15024	0.953

The activation energy (E_a) was calculated from eq. 3, while the corrosion rates (CR_1 and CR_2) were obtained at two different temperatures (308 K and 318 K) for both compounds [28]:

$$E_a = \frac{R \ln \frac{CR_2}{CR_1}}{\frac{1}{T_1} - \frac{1}{T_2}} \quad (3)$$

The activation energy (E_a) can be determined from the slope of log *CR vs.* (1000/*T*) in Fig. 3b. Subsequently, the Arrhenius pre-exponential factor (λ) can be calculated from eq. 4 [27].

$$\log(CR) = \frac{-E_a}{2.303RT} + \lambda \quad (4)$$

The Arrhenius equation (Eq. 5) was used to calculate the thermodynamic parameters such as the entropy of activation ($\Delta S_{ads.}$) and enthalpy of activation ($\Delta H_{ads.}$), where *T* is the temperature in Kelvin, *R* is the gas constant, *N* is the Avogadro constant and *h* is the Plank constant. From the slope and intercept of log (*CR*/*T*) *vs.* (1000/*T*), ΔH and ΔS were calculated from (-ΔH/*2.303R*) and [log(*R*/*Nh*) + (ΔS/2.303*R*)], respectively (Fig. 3b). The calculated thermodynamic parameters are

tabulated in Table 2. These results were compromised with obtained results by numeral researchers such as Rafiquee *et al.*, [11] and Ahamad *et al.*, [29].

It can be observed that **A1** gave higher values of λ, E_a, ΔH and ΔS. These values show that **A1** has better corrosion inhibition performance compared to **A2**. The quantum chemical behavior of inhibitors has been computing using quantum calculating software such as Gaussian [30-32]. In this study, the energy of the highest occupied molecular orbital (E_{HOMO}) and the energy of the lowest unoccupied molecular orbital (E_{LUMO}) were calculated using Gaussian software 9.0. Table 2 shows that the calculated E_{HOMO} and E_{LUMO} are almost the same. However, the largest difference between the energies of E_{HOMO} and E_{LUMO} (ΔE) is exhibited by **A1**. It can be concluded that **A1** has good electron donor properties compared to **A2**. Logically, atoms with more electron charge density can easily be donated to an electron acceptor in the activated sites of the corroding surface. The Frontier Molecular Orbital (FMO) density distributions for **A1** and **A2** are shown in Fig. 4. Based on the FMO results, the inhibition mechanism on the nickel surface can be described.

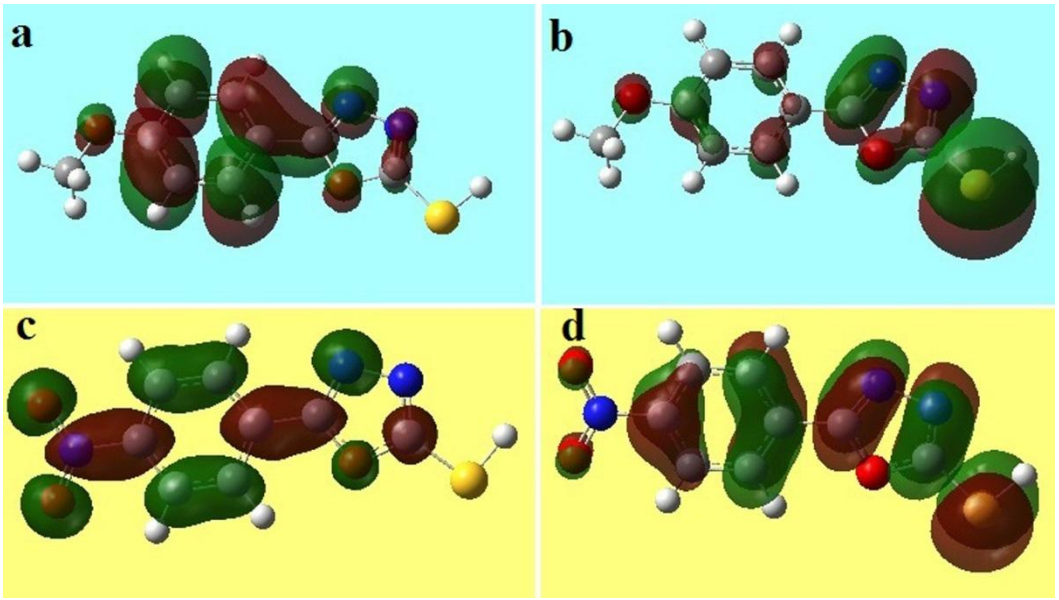

Figure 4. Frontier molecular orbital density distribution for **A1** (a: HOMO, b: LUMO) and **A2** (c: HOMO, d: LUMO).

Table 2. Computational and thermodynamic molecular parameters for the **A1** and **A2** compounds.

Samples	A1	A2
$\Delta S_{ads.}$ (kJ mol^{-1})	-111.99	-127.57
$\Delta H_{ads.}$ (kJ mol^{-1})	36.66	32.11
λ (mg cm^{-2} h^{-1})	-38.4 $\times 10^{+6}$	-52.9$\times 10^{+6}$
E_a (kJ mol^{-1})	43.73 ±0.48	15.72 ±0.55
E_{HOMO} (eV)	-0.2643	-0.2046
E_{LUMO} (eV)	0.1648	0.1413
$\Delta E = E_{LUMO} - E_{HOMO}$	0.4291	0.3459

Figure 5a shows that the methoxy group in **A1** and the nitro group in **A2**, in the benzene ring, are electron donors and electron acceptors, respectively. The electron accepting behavior of the nitro group is due to the higher electro-negative properties of the oxygen and nitrogen atoms. The electron density from the heterocyclic 1,3,4-oxadiazole is transferred to the nitro group *via* the benzene ring. Hence, the performance of **A2** as an inhibitor is decreased (Fig. 5b). The activated sites on the nickel surface can be blocked by one or more of the following behaviors: (I) electrostatic interaction between the charged atoms of the inhibitors and the activated charged metal surface. (II) Unshared electron pairs in the hetero-atoms in the heterocyclic molecules and the metal surface atoms with vacant d-orbitals. (III) Interactions of π-electrons with the metal surface. (IV) Interactions between prorogated inhibitors with pre-absorbed chloride ions. Figure 4b shows that the highest electron density is agglomerated in the **A1** molecule. Figure 5a shows that the electron pairs of the N, S and O atoms from the heterocyclic 1,3,4-oxadiazole are good electron donors to the activated sites on the corroding surface compared to the same atoms in **A2**. The same mechanisms were developed by Ahamad *et al.*, [10] and Yadav et al., [34] while they have used organic molecules as inhibitors for mild steel.

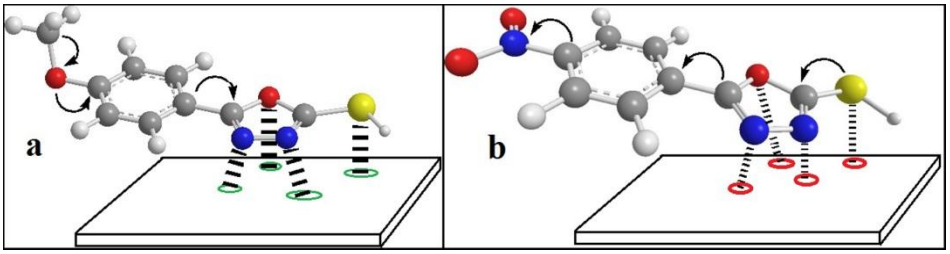

Figure 5. A schematic model for the adsorption of a: **A1** and b: **A2** on the nickel surface in corrosive media.

3.3. Impedance measurements

EIS is a powerful tool that elucidates the kinetics of the corrosion process. The corrosion behavior of nickel foils was examined in uninhibited and inhibited 3.5% NaCl solutions at OCP at room temperature. The most accurate equivalent circuit was obtained from the closest fit of the experimental data with an analogue circuit, with the chi-squared value minimized to 10^{-4}. The results indicate that corrosion occurs *via* a two-step process from the appearance of two time constants (Fig. 6). From the comparison between the simulated and experimental data for Ni corrosion in the presence of **A1** and **A2**, the most accurate equivalent circuit model for the Nyquist plots is $R_s(C_{dl}[R_p(R_{ct}Q)])$. The equivalent circuit model can be described as follows. R_s is the solution resistance between the WE (nickel plate) and the RE (SCE electrode). R_p is the pore resistance, which is due to the corrosion of the Ni surface, resulting in pore formation in the bulk metal. C_{dl} is the double layer capacitance of the pores from the intake of water and ions into the pores, where R_p and C_{dl} form the first parallel combination. The second parallel combination consists of the charge transfer resistance (R_{ct}) and the constant phase element (CPE), which is in series with R_p. Instead of the pure capacitance (C), the CPE (denoted as Q in the circuit) is introduced in the simulation process to obtain good agreement between

the simulated and experimental data. The CPE impedance is defined as $Z_{CPE} = [Q(i\omega)^n]^{-1}$, where Q (Ω^{-1} s^n cm^{-2}) is the combination of properties related to the surface and electroactive species independent of frequency [14]. Thus, Q will be closer to the capacitance if "n" is closer to 1. The "n" value also depends on the surface roughness. The charge transfer resistance R_{ct} is another parameter that provides information about the electron transfer process; thus, the R_{ct} value is a measure of the corrosion reaction that occurs across the Ni electrode/electrolyte interface [34].

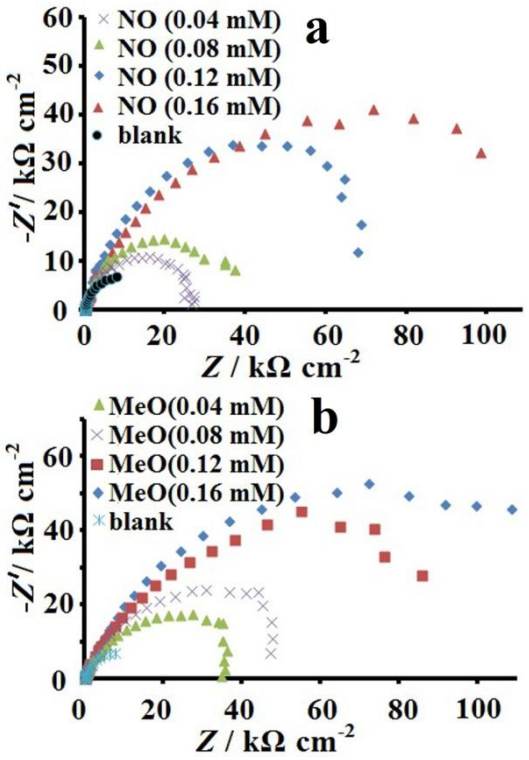

Figure 6. Nyquist plots (vs. SCE) for nickel plates immersed in various amounts of a: **A2** and b: **A1** compounds in 3.5% NaCl.

Parameters such as R_s, C_{dl}, R_{ct}, Q and n are tabulated in Table 3. It can be observed that the Q and C_{dl} values increase with increasing inhibitor concentration (**A1** and **A2**) in the corrosive media, leading to an increase in inhibitor adsorption on the corroding surface. From the Nyquist plots of both inhibitors in the corrosive media, **A1** has a larger semi-circle diameter than does **A2** at the same inhibitor concentration (Fig. 6a and b). The R_{ct} values are tabulated in Table 3, and the R_{ct} for **A1** is 144.2 kΩ cm^2, compared to 119.3 kΩ cm^2 for **A2**, at an inhibitor concentration of 0.16 mM.

Table 3. EIS simulation of the Ni surface in 3.5% NaCl in the presence of different inhibitor concentrations.

Elements→ Inhib.↓	Inhi. Conc. (mM l^{-1})	R_s (Ω cm^2)	R_{ct} (kΩ cm^2)	n	Q mS.s^n. cm^{-2}	C_{dl} (μF cm^{-2})
Blank	0.0	0.229	9.13	0.7012	0.166×10^{-3}	80.7
	0.04	0.731	38.7	0.7008	1.44×10^{-4}	4.86

A1	0.08	0.867	51.7	0.7107	0.291×10^{-4}	4.36
	0.12	1.067	126.2	0.7270	0.366×10^{-4}	6.06
	0.16	1.626	144.2	0.7034	0.251×10^{-4}	8.32
A2	0.04	1.019	29.21	0.729	0.198×10^{-4}	4.40
	0.08	1. 151	39.8	0.721	0.144×10^{-4}	5.97
	0.12	1.701	95.4	0.741	0.235×10^{-4}	6.95
	0.16	2.395	119.3	0.769	0.291×10^{-4}	7.20

3.4. FESEM analysis

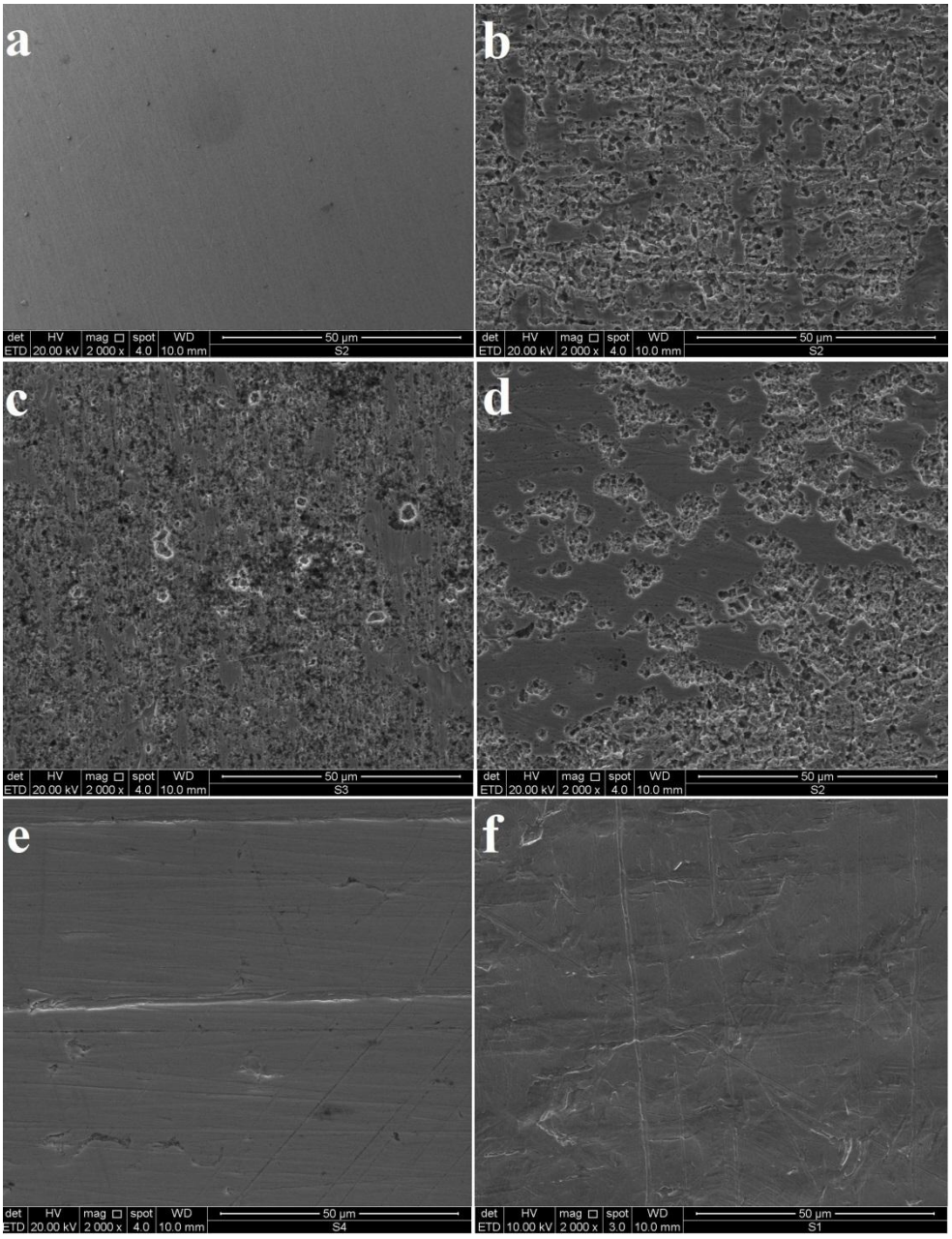

Figure 7. FESEM images of the Ni surface before immersion in 3.5% NaCl (a), after immersion in 3.5% NaCl solution for 30 days with the absence of inhibitors (b), and in the presence of inhibitors: 0.02 mM **A1** (c) and 0.02 mM **A2** (d), 0.3 mM **A1** (e) and 0.3 mM **A2** (f).

The FESEM images in Fig. 7 (a-f) show the effect of the inhibitors **A1** and **A2** on the Ni surface. Figure 7a shows a polished nickel surface that was not immersed in the corrosive media. Figure 7b-f show FESEM images of the nickel surfaces that were immersed in 3.5% NaCl (7b), 3.5% NaCl + 0.02 mM (**A1**: 7c and **A2**: 7d) and 3.5% NaCl + 0.3 mM (**A1**: 7e and **A2**:7f) for 30 days. Figure 7b shows that the Ni surface was vigorously corroded in the absence of inhibitors. It can be observed that the Ni surface was well protected from corrosion due to the increase in inhibitor concentration (7c to 7e: **A1**, 7d to 7f: **A2**).

4. CONCLUSIONS

The EIS, OCP and LSV measurements showed that both **A1** and **A2** performed well in inhibiting nickel corrosion in a 3.5% NaCl solution. The OCP measurements showed that the OCP moves towards more noble potentials with increasing inhibitor concentration. The LSV results showed that the surface convergence (θ) increased to 0.966 and 0.953 for **A1** and **A2**, respectively, at an inhibitor concentration of 0.12 mM in corrosive solution. It can be concluded that the methoxy group in **A1**, which is an electron donor, has better corrosion resistance performance compared to the electron withdrawing group of nitrogen dioxide in **A2**. The charge transfer resistance increased to 144.2 and 119.3 kΩ cm^2 for **A1** and **A2**, respectively, at an inhibitor concentration of 0.12 mM.

ACKNOWLEDGMENTS
This work was supported by grants from the Institute of Research Management and Monitoring PPP grant (PG015-2013A) and (PG084-2013A), a High Impact Research grant (UM.C/HIR/MOHE/SC/37) F000009-21001 and a UM Research Collaborative Grant Scheme (CG045-2013A).

References

1. Z. Jin, *Mat. Prod. Rep.*, 20 (2003) 584.
2. L. D. Quin and J. A. Tyrell, *Fundamentals of heterocyclic chemistry: importance in nature and in synthesis of pharmaceutical.* Hoboken; John Wiley & Sons Inc., (2000).
3. P. M. Dewick, 3rd edn. *Medicinal Natural Products. A Biosynthetic Approach.* United Kingdom: John Wiley & Sons Inc., (2009).
4. P. J. Martin and D. W. Bruce, *Liq. Cryst.* 34 (2007) 767.
5. K. A. Milinkevich, C. L. Yoo, T. C. Sparks, B. A. Lorsbach and M. J. Kurtin, *Bioorg. Med. Chem. Lett.*, 19 (2009) 5796.
6. A. R. Katrizky, P. P. Mohapatra and L. Huang, *Arkivoc*., 9 (2008) 62.
7. V. Summa, A. Petrocci, F. Bonelli, B. Crescenzi and M. Donghi, *et al, J. Med. Chem*., 51 (2008) 5843.
8. M. Ebadi, W. J. Basirun, Y. Alias, M. R. Mahmoudian and S. Y. Leng, *Mater. Charact.*, 66 (2010) 46.
9. M. Ebadi, W. J. Basirun, S. Y. Leng and M. R. Mahmoudian, *Int. J. Electrochem. Sci.*, 7 (2012) 8052.
10. I. Ahamad, R. Prasad and M. A. Quraishi, *Corros. Sci*., 52 (2010) 1472.
11. M. A. Rafiquee, S. Nidhi, K. Sadaf and M. A. Quraishi, *Mater. Chem. Phys*., 107 (2008) 528.
12. E. M. Sherif and Su-M. Park, *Electrochim. Acta.*, 51 (7), (2006) 1313.

13. M. Ehteshamzadeh, T. Shahrabi and M. Hosseini, *Anti-Corros. Meth. Mater*., 53 (5) (2006) 296.
14. A. A. Nazeer, A. S. Fouda and E. A. Ashour, *J. Mater. Environ. Sci.*, 2 (1) (2011) 24.
15. J. B. Matos, L. P. L. Pereira, S. M. Agostinho, O. E. Barcia, G. G. O. Cordeiro and D'. E. Elia, *J. Electroanal. Chem*., 570 (1) (2004) 91.
16. T. Fallavena, M. Antonow and R. S. Goncalves, *Appl. Surf. Sci*., 253 (2) (2006) 566.
17. S. Rajendran, S. Vaibhavi, N. Anthony and D. C. Trivedi, *Corr. Sci*., *59* (6) (2003) 529.
18. M. R. Mahmoudian, W. J. Basirun, Y. Alias and M. Ebadi, *Appl. Surf. Sci*., 257 (20) (2011) 8317.
19. M. G. Mahjani, M. Sabzali, M. Jafarian and J. Neshati, *Anti-Corros. Meth. Mater.*, 55 (4) (2008) 208.
20. M. Ebadi, W. J. Basirun, Y-L. Sim and M. R. Mahmoudian, *Metall. Mater. Trans. A*, 44 (2013) 5096.
21. A. Hasan, N. F. Thomas and S. Gapil, *Molecules*., 16 (2011) 1297.
22. A. Hasan, M.R.K. Sheikh and S. Gapil, *Asian J. Chem*., 24 (6) (2012) 2573.
23. E. S. Ferreira, C. Giancomelli, F.C. Giacomelli and A. Spinelli, *Mater. Chem. Phys.*, 83 (2004) 129.
24. H. A. El-Dahan, T. Y. Soror and R. M. El-Sherif, *Mater Chem Phys.*, 89 (2005) 260.
25. M. Ebadi, W. J. Basirun, H. Khaledi and H. M. Ali, Chem. *Cent., J.*, 6 (2012) 163.
26. I. Ahamad, R. Prasad and M. A. Quraishi, *J. Solid. State. Electrochem*., 14 (2010) 2095.
27. A. K. Singh, S. K. Shukla, M. Singh and M. A. Quraishi, *Mater. Chem. Phys*., 129 (2011) 68.
28. http://www.chem1.com/acad/webtext/dynamics/dynamics-3.html
29. I. Ahamad, R. Prasad and M.A. Quraishi, *Corro. Sci.*,52 (2010) 933.
30. J. Cruz, E. Garcia-Ochoa and M. Castro, *J. Electrochem. Soc.*, 150(1) (2003) B26.
31. I. Danaee, O. Ghasemi, G.R. Rashed, M. Rashvand Avei and M.H. Maddahy, *J. Molecul.* Struc., 1035 (13) (2013) 247.
32. A. Döner, R. Solmaz, M. Özcan and G. Kardas, *Corro. Sci.*, 53 (9) (2011) 2902.
33. D, K, Yadav, B. Maiti and M.A. Quraishi, *Corr. Sci.*, 52 (2010) 3586.
34. M. Keddam, O. R. Mattos and H. Takenouti, *J. Electrochem. Soc.*, 81 (8) (1981) 7.